ASSESSING THE INTERACTION OF A LASER BEAM AND POLYMERIC POWDERS IN POLYMER LASER SINTERING

Fredrick Mwania[1], Maina Maringa[2] *and* Jacobus van der Walt[3]

[1] Department of Mechanical and Mechatronic Engineering Central University of Technology, 20 President Brand Street, Bloemfontein, South Africa, *Corresponding author*, ORCID No. 0000-0001-8702-2496, fredmulinge@gmail.com
[2] Department of Mechanical Engineering, Múrang'a University of Technology, P. O. Box 75-10200 Múrang'a, Kenya, ORCID No. 0000-0002-8965-1242, maringa@mut.ac.ke
[3] Department of Mechanical and Mechatronic Engineering Central University of Technology, 20 President Brand Street, Bloemfontein, South Africa, ORCID No. 0000-0001-8323-343X, jgvdwalt@cut.ac.za

ABSTRACT: Polymer laser sintering (PLS) has received considerable attention for the last four decades. However, some of its aspects are not well understood to date. This study aims to shed light on the complex interaction between a laser beam and polymeric powder particles during sintering, which is a critical stage in PLS. In this work, an analytical model linking the degree of fusion of particles of powder with their material properties together with process-parameters was developed using dimensional analysis and the Buckingham *Π* theorem. It was proved using experimental data that the developed analytical model can be used to optimise different process-parameters by establishing a set of parameters providing the highest value of a proposed parameter to represent the degree of fusion of particles (Ω). This value for polypropylene powder (Ultrasint PP nat 01 from BASF) was approximated as 0.25, based on suitable process-parameters. Numerical modelling was conducted using Flow 3D software to investigate the characteristics of depth and width of a melt pool because these aspects are essential indicators of the stability of PLS and the quality of the final parts printed using polymer laser sintering. The obtained simulation results showed that melt pool width and depth increased with increasing laser power and decreased with increasing scanning speed.

KEYWORDS: *polymer laser sintering; analytical model; degree of fusion; process-parameters; material properties*

1. INTRODUCTION

A laser beam is used to melt and fuse powder materials in PLS. In this process, particles of powder are first pre-heated to a temperature close to their melting point before exposure to a laser beam [1]. Strategically placed heaters are used to pre-heat powder in the build chamber to a predefined temperature, which is close to the melting point of the material for semi-crystalline polymers and to glass transition temperature for amorphous polymers [2, 3]. A laser beam, mostly a CO_2 laser beam, provides the extra energy after this preheat session, that is needed to melt the grains of polymer, which allows them to fuse once their surface tension has been overcome [1]. The process of consolidation of particles of powder in PLS is illustrated in Figure 1. It involves the three steps of surface contact, formation of a neck, and growth of a neck. According to Franco *et al*. [4] coalescence of polymer particles, during sintering, is a sophisticated process. However, understanding this process is essential because it defines the properties of the final parts produced through sintering [5, 6, 7, 8]. Hence, the development of models to describe sintering and fusion of particles is indispensable when modelling PLS.

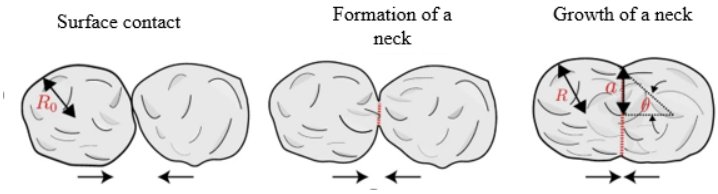

Figure 1. Fusion of particles of powder in PLS [9]

According to Mokrane *et al*. [10], the sintering process involves interaction of a laser beam and powder in the build chamber, melting of powder, and densification of particles. This involves changes of the thermo-physical properties of melting zones, which influence the density and micro-structure of printed parts. Considerable work has been carried out to model the interaction of laser beams and polymeric powders. Some of the notable works include those of Zhang *et al*., [8]; Mokrane *et al*., [10]; Gusarov and Smurov [11]; Yaagoubi *et al*., [12]; and Yaagoubi *et al*. [13]. Most of these studies attempted to show that sintering of particles of powder can be assessed using

numerical modelling, but they did not address the aspect of optimising process-parameters. Therefore, more effort should still be directed to this area to provide useful insights into the phenomenon of fusion of powder, with the aim of also facilitating optimisation of the process-parameters for different polymeric feedstock materials, especially those factors related laser energy density.

Laser energy densities are crucial because they influence the fusion of particles, which affects the mechanical properties of printed parts [14]. Mathematical expressions have been developed to calculate laser energy densities, as shown by Equations 1, 2, and 3, which represent linear or 1D energy density (LED), area or 2D energy density (AED) and volumetric or 3D energy density (VED), respectively [15]. The three formulas are normally used to optimise the different process-parameters of laser power, laser scanning-speed, hatch spacing, and layer-thickness. However, Hofland *et al*. [16] showed fusion of particles to be dependent on the total energy absorbed by them, which includes energy from both pre-heating and the laser beam. The energy due to the preheating can be calculated using Equation 4. Equation 5 sums up the energy absorbed by powder due to a pre-heating process and its interaction with a laser beam. Though Equation 5 is not commonly used to optimise process-parameters in PLS, it is recommended, in this study, to adopt the equation because it considers preheating, which should not be ignored.

$$LED = \frac{P}{v} \quad (1)$$

$$AED = \frac{P}{v \times h} \quad (2)$$

$$VED = \frac{P}{v \times h \times t} \quad (3)$$

$$E_p = C_p \times \rho \times \Delta T \quad (4)$$

$$E_T \approx \left[\frac{P}{v \times h \times t}\right] n + \left[C_p \times \rho \times \Delta T\right] \quad (5)$$

where,

LED = linear energy density (J/mm), AED = area energy density (J/mm^2)
VED = volumetric energy density (J/mm^3), P = laser power (W), v = scanning-speed of the laser beam (mm/s), h = hatch spacing (mm), t = powder layer-thickness (mm), E_p = energy absorbed by powder due to the preheating process (J), C_p = specific heat capacity of the material $(J/kg.K)$, ρ = bulk material density (kg/m^3), ΔT = Preheating change in temperature (preheating temperature – room temperature) (K), E_T = Total energy absorbed by powder due to pre-heating and interaction with the laser beam (J), n = number of runs of a laser beam

Various studies have been undertaken to investigate how the absorption of energy affects interlayer and intra-layer fusion during sintering [1, 3, 17]. However, there is information that is still missing, especially on the aspect of optimisation of different process-parameters and material-properties. The mentioned studies [1, 3, 17] illustrated that the phenomenon of sintering in PLS can be investigated using numerical analysis, but they did not illustrate how this assessment can be employed to optimise different process-parameters, such as laser power, scanning-speed, or hatch spacing. Hence, the need for further development of new or improvement of existing models to describe the absorption of energy by particles of powder and their subsequent fusion. These new or improved models are expected to provide crucial information, such as depth of penetration and levels of fusion that can be used to optimise different process-parameters, thus, promoting good interlayer and intra-layer fusion of particles, and reduction of pores. Therefore, it is crucial to understand well how the total energy absorbed by particles in PLS impact on the melt-pool using either analytical, experimental or numerical techniques.

Experimental, analytical, and numerical investigations of laser beam-powder interactions can help enhance the understanding of PLS. This is expected to lead to better optimisation of process-parameters and a better understanding of how material-properties of powders impact on the process, both which are the key factors affecting the success of PLS [18]. The experimental approach of optimising process-parameters for new materials is time-consuming, complex, and costly, particularly when applied to different powders and different PLS machines [19]. Analytical and numerical modelling are cheaper and less time-consuming alternatives. While various models have been used to investigate the degree of fusion of particles in PLS [1, 3], few studies have linked this phenomenon to the material-properties of powders and process-parameters. Based on the sintering conditions and the materials properties of powders, sintered particles can undergo partial or full sintering. Incomplete sintering and particle fusion are not desirable because they lead to

poor mechanical properties of sintered parts [20]. Therefore, it is essential for more research to be directed to the interaction of the laser beam and powder. Analytical models were developed in the present research that can be used to investigate the phenomenon of fusion of particles in PLS, taking due account of the material properties of powders and process-parameters. Numerical modelling was also undertaken to examine the influence of different process-parameters on the melt pool characteristics of a polypropylene powder with the aim of assessing suitability of Flow 3D software for simulating PLS.

2. EXPERIMENTAL INVESTIGATION TO STUDY FUSION OF PARTICLES OF POWDER

An experimental investigation was conducted to examine the fusion phenomenon of particles of powder, which was then used to select the best analytical model to describe the sintering process in PLS carried out in the present work. Hot stage microscopy was undertaken using a HFS91 microscope. Images were captured in this process using ScopePhoto software 3.1, which involved a set-up process with the following steps (Acquire – Twain Aquire – Framtech USB PC camera). The format of the images was selected as JPEG with an output size of 640 × 480 pixels. The sample of powder used was spread and sandwiched between two glass cover slides and placed on the sample holder. The behaviour of the particles of powder was observed at different temperatures, and images obtained for analysis. Hot stage microscopy was carried out in recognition of the fact that it is an important tool for validating crucial numerical models for PLS on the basis of, fusion of particles, impact of different cooling rates, and effect of high packing density and uniformity of the powder bed.

As mentioned earlier in this study, the degree of fusion of particles is pivotal to the success of PLS and also determines the quality of finished parts [10]. The fusion behaviour of polymeric materials can be assessed experimentally using hot stage microscopy. The obtained results can also be used to validate analytical and numerical models for particle-fusion, which is the basis for PLS. In the present work, hot stage microscopy was used to investigate the fusion of particles of Ultrasint PP nat 01, with the results shown in Figure 2.

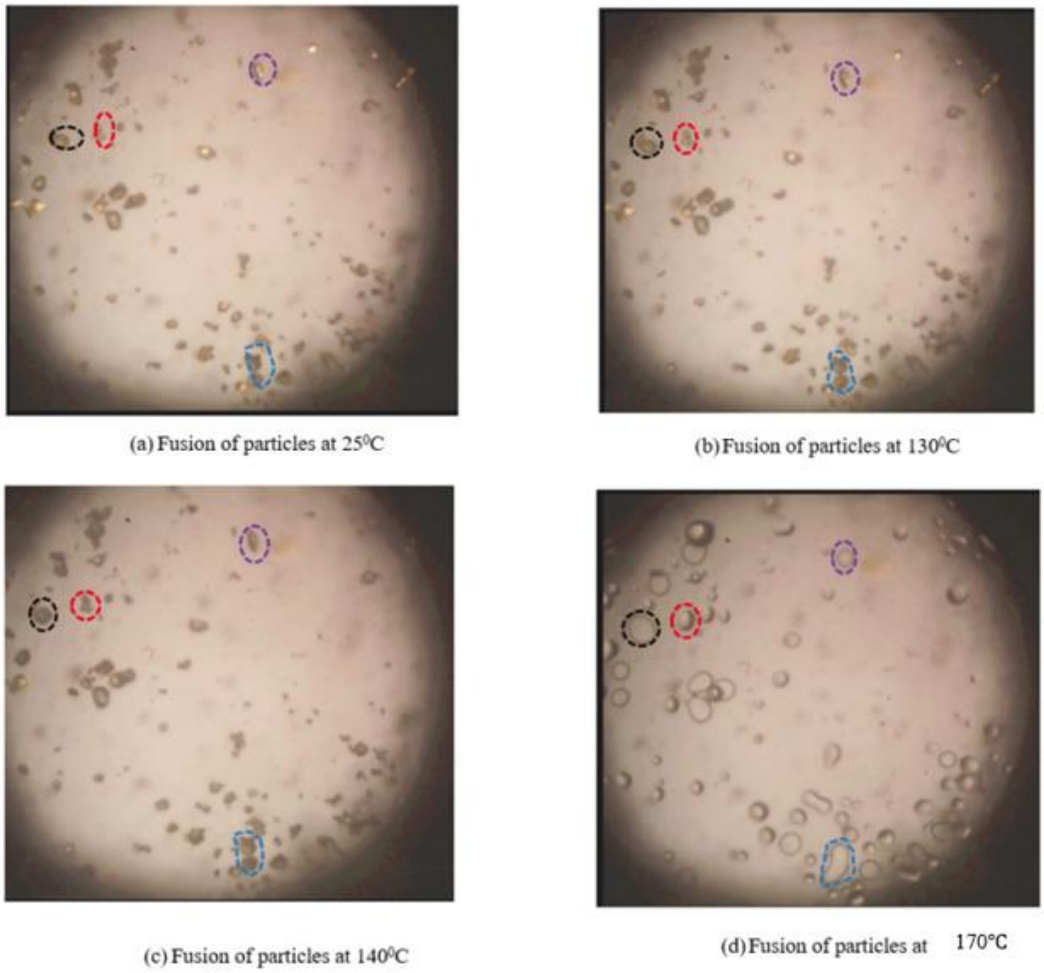

(a) Fusion of particles at 25^{0}C

(b) Fusion of particles at 130^{0}C

(c) Fusion of particles at 140^{0}C

(d) Fusion of particles at 170°C

Figure 2. Fusion of particles of Ultrasint PP nat 01 at different temperatures

The behaviour of different sets of particles (encircled using black, red, purple, and blue circles) was examined at 25, 130, 140, and 180 °C. The obtained results illustrated that the particles started to melt and fuse at 140 °C (as the particles started to merge), and full fusion was attained at 170 °C. The data also showed that Ultrasint PP nat 01 has good wetting properties since some of the particles (the particles encircled by red, black, and purple circles) were able to attain almost a perfect circular shape at the end of the sintering process at 170 ^{0}C. Such results can be used to validate analytical and numerical models illustrating fusion of particles and wetting properties of different polymers at different temperatures. The temperature at which full fusion is attained is also a critical factor that can be used to optimise volumetric laser energy density, which contains the most crucial process-parameters of laser power and scanning-speed in PLS. The results also indicated that the fusion of particles increased with temperature, which can be taken to imply that the phenomenon of coalescence of particles is subject to the total energy absorbed by them. Hence, the energy from the pre-heating phase in PLS should be considered when developing analytical models to establish total energy absorbed by particles of powder. This information was considered when selecting the best analytical model to represent fusion of particles during sintering in PLS.

3. DEVELOPMENT OF ANALYTICAL MODELS TO INVESTIGATE THE PHENOMENON OF FUSION OF PARTICLES OF POLYMER POWDER IN POLYMER LASER SINTERING

Benedetti *et al*. [21] stated that the study of the coalescence of particles of powder in PLS is crucial because it provides essential information on the mechanisms of consolidation of the powder. According to Lupone *et al*. [3], various models have been developed to predict the coalescence behaviour of viscous materials. The Frenkel's model, which is the most commonly utilised one is as represented in Figure 3 and by Equation 6.

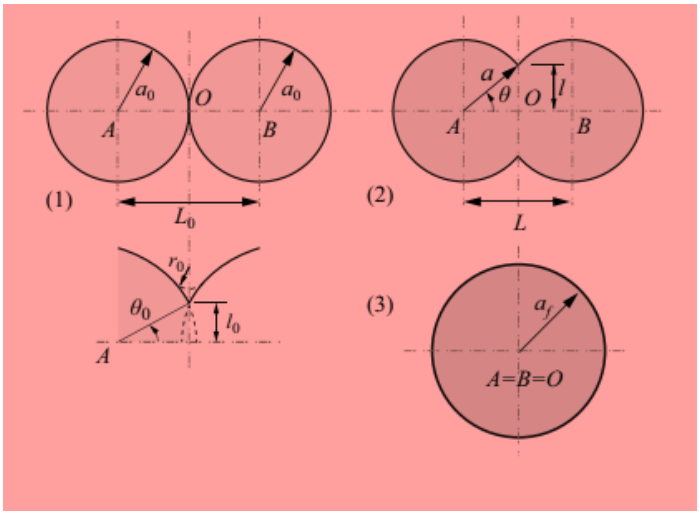

Figure 3. The coalescence of particles according to Frenkel's model [22]

$$\left(\frac{2l}{d_i}\right)^2 = \frac{\gamma}{\eta a_0} T \tag{6}$$

The degree of fusion ($\propto$) of particles for the case of PLS can be expressed as function of the ratio ($2l/d_i$) in Equation 7, whereby the higher the ratio, the higher the degree of fusion and vice versa.

$$(\propto) = f\left(\frac{2l}{d_i}\right)^2 = \frac{\gamma}{\eta a_0} T \tag{7}$$

where,

l = neck radius (m)

d_i = diameter of fused particles at room temperature (m)

γ = surface tension (N/m)

η = viscosity ($kgm^{-1}s^{-1}$)

a_0 = initial radius of the particles (m)

T = sintering time (s)

Equations 6 and 7 only use materials properties, without considering the process-parameters. This study aims to link the fusion of particles of polymer to the PLS process-parameters and material-properties. Dimensional analysis and the Buckingham Π theorem were used to develop a model describing fusion of particles of powder, as outlined below this paragraph. The following pertinent process-parameters and the material-properties were considered in this case: degree of fusion ($\propto$) bulk material density (ρ), surface tension (γ), viscosity (η), sphericity (k), average size of

particles (d), and total energy absorbed by particles of powder (E_T).

Number of relevant factors (n) = 7

Dimensions of the identified variables: $\propto$ $=dimensionless\ num$ $\rho = ML^{-3}$, $\gamma = MT^{-2}$, $\eta = ML^{-1}T^{-1}$, $k = dimensionless\ number$, $d = L$, $E_T = ML^2T^{-2}$

Number of base dimensions (m) = 3

Recurring variables: (ρ, γ, d)

Number of non-dimensional pi-groups: $k = n - m = 7 - 3 = 4$

Creating the first pi-group Π_1:

$$\Pi_1 = \propto$$

Creating the second pi-group Π_2:

$$\Pi_2 = \eta/\rho^a\gamma^b d^c$$

$$ML^{-1}T^{-1} = (ML^{-3})^a\ (MT^{-2})^b(L)^c$$

Equating the base dimension of mass, length and time on the left of this equation to those on the right leads to the expressions:

$1 = a + b$, *from the base dimension of mass (M)*

$-1 = -3a + c$, *from the base dimension of length (L)*

$-1 = -2b$, *from the base dimension of time (T)*

Solving for a, b, and c; $a = b = c = \frac{1}{2}$

Therefore,

$$\Pi_2 = \eta/\sqrt{\rho\gamma d}$$

Creating the third pi-group Π_3:

$$\Pi_3 = E_T/\rho^a\gamma^b d^c$$

$$ML^2T^{-2} = (ML^{-3})^a\ (MT^{-2})^b(L)^c$$

Equating the base dimension of mass, length and time on the left of this equation to those on the right leads to:

$1 = a + b$, *from the base dimension of mass (M)*

$2 = -3a + 2c$, *from the base dimension of length (L)*

$-2 = -2b$, *from the base dimension of time (T)*

Solving for a, b, and c; $a = 0$, $b = 1$, *and* $c = 1$

Therefore,

$$\Pi_3 = E_T/\gamma d$$

Creating the fourth pi-group Π_4:

$$\Pi_4 = k$$

Setting out the non-dimensional relationship for these four pi-groups:

$$\Pi_1 = f(\Pi_2, \Pi_3, \Pi_4)$$

It is important to note that the second, third and fourth pi-groups each contribute to the degree of fusion ($\propto$) based on different considerations and my thus be written as:

$$\propto_{\pi_2} = f\left(\frac{\eta}{\sqrt{\rho\gamma d}}\right) \quad (8)$$

$$\propto_{\pi_3} = f\left(\frac{E_T}{\gamma d}\right) \quad (9)$$

$$\propto_{\pi_4} = f\ (k) \quad (10)$$

The total energy absorbed by particles of powder can be approximated using the following proposed analytical model (Equation 11), obtained from Equation 5, provided in the background section.

$$E_T \approx \left[\frac{P}{v \times h \times t}\right] n\ +\ \left[C_p \times \rho \times \Delta T\right] \quad (11)$$

where,

E_T = Total energy absorbed by the powder due to the pre-heating process and interaction with the laser beam (J)

P = laser power (W)

v = speed of the laser beam (m/s)

h = hatch spacing (m)

t = powder layer-thickness (m)

n = number of laser beam exposures

C_p = specific heat capacity of the material ($J/kg.K$)

ρ = bulk material density (kg/m^3)

ΔT = change in temperature (preheating temperature – room temperature) (K)

Equations 8, 9, 10 illustrate that the degree of fusion is subject to melt viscosity, bulk material density, surface tension of the melt, size of particles (represented by the mean diameter), total energy absorbed by the powder due to the pre-heating process and the interaction of the laser beam with particles of powder, and particle sphericity. Equation 9 can be used to investigate how different process-parameters, provided in Equation 11, affect the degree of fusion of particles. Equations 8 and 10 were disregarded in this study because they do not consider the total energy absorbed by the particles of the powder, which is the focus of the optimisation process considered here, but it is recommended that they be investigated in future studies. A parameter (Ω) is now defined to represent the degree of fusion of particles based on Equation 9, as shown in Equation 12.

$$\Omega \approx \frac{\left[\left[\frac{P}{v \times h \times t}\right] n + \left[C_p \times \rho \times \Delta T\right]\right]}{\gamma d} \quad (12)$$

where,

Ω = a parameter to represent degree of fusion of particles

P = laser power (W)

v =scanning space (mm/s)

h = hatch spacing (mm)

t = powder layer-thickness (mm)

n = number of laser beam exposure

C_p = specific heat capacity of the material ($J/g\ K$)

ρ = bulk material density (kg/m^3)

ΔT = change in temperature (preheating temperature – room temperature) (K)

γ = surface tension (N/m)

d = average particle size (m)

Equation 12, was used to estimate the parameter Ω for polypropylene (Ultrasint PP nat 01) powder using results from a previous study [23] and with values of the parameters shown below [23]:

$P = 44.8\ W$

$v = 4500\ mm/s$

$t = 0.15\ mm$

$h = 0.35\ mm$

$C_p = 2.381\ J/g\ K$ [24]

$\rho = 0.370\ g/cm^3$ (0.00037 g/mm^3)

$\Delta T = 100\ K$

$\gamma = 24.7\ mN/m$ [25]

$d = 0.045\ mm$

Thus, giving rise to:

$$\Omega \approx \frac{\left[\left[\frac{44.8}{4500 \times 0.35 \times 0.15}\right] 1 + [2.381 \times 0.00037 \times 100]\right]}{(24.7 \times 0.045)} = 0.25$$

For a given set of parameters, the values that yielded the highest value of Ω were taken to be the most suitable, because this denoted the highest degree of fusion of the particles of powder.

The accuracy of the developed analytical model (Equation 12) was tested using experimental data obtained from previous work [26] by the authors, that was conducted to examine the best volumetric energy density of Diapow PP MF PP material by dynamic mechanical analysis. In this study, the process-parameters outlined in Table 1 were considered. The values of C_p, ρ, ΔT, γ, and d were taken from [24, 25, 26] as 2.381 $J/g\ K$, 0.00045 g/mm^3, 100 K, 24.7 mN/m, and 0.050 mm, respectively. The values for specific heat capacity of the material and surface tension taken as for neat PP as provided in [24] and [25], respectively. Manufacturer's values were considered for the other factors, as given in [26]. These parameters were used to calculate different values of Ω using Equation 12. The results arising from these calculations are summarised in Table 1.

Table 1. Calculated values of Ω of Diapow PP MF PP for different process-parameters

#	Laser power (W)	Scanning speed (mm/s)	Layer-thickness (mm)	Hatch-spacing (mm)	Calculated (Ω)
1	32.9	5000	0.15	0.30	0.21
2	32.9	4800	0.15	0.30	0.21
3	32.9	4500	0.15	0.30	0.22
4	32.9	4000	0.15	0.30	0.23
5	32.9	3800	0.15	0.30	0.24
6	32.9	3700	0.15	0.30	0.25
7	32.9	3600	0.15	0.30	0.26
8	32.9	3500	0.15	0.30	0.27
9	35.0	3500	0.15	0.30	0.32
10	32.9	3000	0.15	0.25	0.34

According to the study by Mwania *et al*., [26], the best process-parameter set of laser power, scanning speed, layer thickness, and hatch distance, to produce parts with low damping and high static load carrying capacity were determined to be 32.9 W, 3000 mm/s, 0.15 mm, 0.25 mm, respectively (volumetric laser energy density = 0.290 J/mm ^{3}). These process-parameters are seen in the preceding table to have yielded the highest value of Ω. Thus, the developed analytical model can be used to estimate the best process-parameters for polymeric materials in PLS, by selecting the set of process-parameters that yield the highest value of Ω.

4. NUMERICAL MODELLING OF THE FUSION PHENOMENON IN PLS USING FLOW 3D SOFTWARE

Numerical analysis was undertaken to investigate a single track after scanning using a laser beam. The developed numerical model was used to investigate the impacts of laser power and scanning-speed on melt pools. Numerical modelling began by simulation of a single track on a powder bed developed after spreading of powder. The particle to STL converter module was used to convert data obtained from the spreading simulation to an STL file. After this, a new simulation, labelled melting, was added in the Flow 3D setup. The unit system was changed to CGS (centimetre, gram, second) and temperature into Kelvin. In the global icon, found in the model setup tab, the finish time for simulation time was set to 0.0005 seconds. Relevant physics models needed for the simulations was added in the physics icons, which is found below the global icon (Figure 4). The models considered included bubble and phase change, heat transfer, evaluation of density, gravity and non-inertial reference, solidification, surface tension, and viscosity.

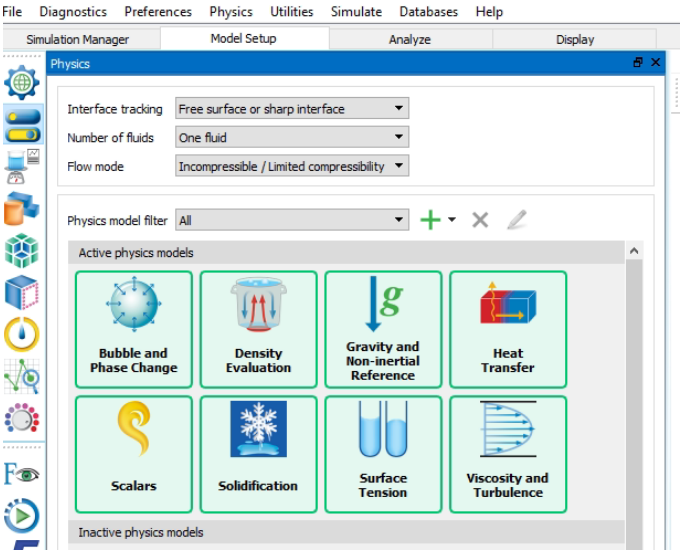

Figure 4. Relevant physics models required to run a PLS simulation in Flow 3D software

Once, all the relevant physics models had been activated, the properties of the material were defined in the Fluids icon. The properties of the material were then entered manually because the software does not have pre-defined properties for polymers in its library. The laser parameters were set using Flow 3D Weld, where the position, laser power, scanning-speed, and spot diameter of the beam were defined.

4.1 Models and properties of the material

4.1.1 Models considered in the simulation

Constant pressure bubbles with vaporisation was considered in this analysis. The other aspects specified in this model are summarised in Table 2.

Table 2. Parameters described in the bubble and phase change model

Parameter	Values obtained from literature
Ratio of specific heats for vapour	1.15
Pressure	1.0e+06 dyne/cm^2
Heat transfer to void type 1	1.0e+05 erg/s/cm^2/K
Accommodation coefficient for evaporation	0.51

The ratio of specific heats for polypropylene vapour was taken as 1.15 based on information obtained from FLSMIDTH [27]. Atmospheric pressure was used to represent the void pressure (the pressure within the build chamber) for the reason that sintering within the build chamber occured at atmospheric pressure. The highest possible convective heat transfer coefficient for air under forced convection was selected as suggested by the FLOW 3D support, because of the relatively high temperature environment in the build chamber. A first order heat transfer model was selected and implicit numerical approximation considered to simplify the process being modelled and reduce the computation time without affecting the accuracy of the obtained results. Gravity was activated to prevent powder particles from flying out of the simulation domain, and the value in Z-direction was set as -981 cm/s^2. The solidification model was activated and the no-shrinkage option selected due to limitations of the software. The solidification model allows the melt pool to cool down and solidify after sintering. A value of the accommodation coefficient for polypropylene could not be found in literature. Hence, a novel approach was adopted to determine it in this work, that involved using thermogravimetric analysis (TGA) as described in the ensuing discussion, from which a value of 0.51 was calculated.

In this particular analysis, TGA for the selected polypropylene material (Ultrasint PP nat 01 powder) was conducted using an STA 6000, PerkinElmer Thermal Analyser. Around 17 milligrams of powder was placed in a crucible and then heated from 30.0 °C to 665.0 °C at 10.0 °C/min, with a one minute hold at 30.0 °C. The experiment was undertaken in an atmosphere of nitrogen. The TGA graph shown in Figure 5 was obtained, in which it is evident that the material began to disintegrate at a temperature of 258 ℃, and broke-down completely at a temperature of 453 ℃. The curve between the onset and terminal degradation temperatures in Figure 5 was used to determine the accommodation coefficient for polymeric materials, as is normally done when undertaking numerical simulations in Flow 3D software, as illustrated in Equation 13.

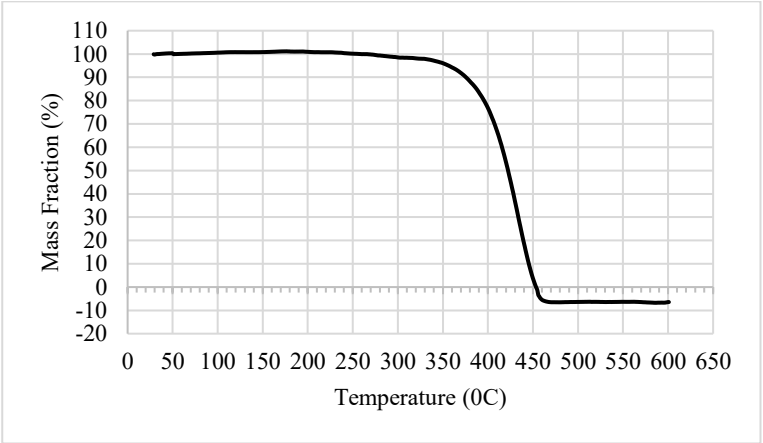

Figure 5. TGA curve for fresh Ultrasint PP nat 01 powder

$$\text{Accommodation coefficient} = \frac{M_o - M_f}{T_o - T_f} \qquad (13)$$

where,

M_o = Mass fraction at the onset of degradation

M_f = Mass fraction at the end of degradation

T_o = Onset degradation temperature

T_f = Terminal degradation temperature

Substituting the values of the foregoing parameters obtained from the TGA curve that was plotted in the present work led to:

$$\text{Accommodation coefficient} = \left|\frac{99.988 - 0.507}{257.89 - 452.89} = 0.51\right|$$

4.1.2 Density

Density was considered to be a function of temperature. The values of density used in this study, outlined in Table 3, were obtained from a previous investigation by Lazar et *al*., [28].

Table 3. Polymer melt density at different temperatures [28]

Temperature (℃)	Temperature (K)	Density (g/cm^3)
180	453	0.876
190	463	0.881
200	473	0.884
210	483	0.891
220	493	0.898
230	503	0.910
240	513	0.916
250	523	0.918
260	533	0.922

4.1.3 Surface tension

Surface tension was defined as a function of temperature as outlined in Table 4.

Table 4. Surface tension of PP at different temperatures [29]

Temperature (°C)	Temperature (K)	Surface tension (mN/M)	Surface tension (g/s^2)
180	453.15	20.57	20.57
190	463.15	20.02	20.02
200	473.15	19.59	19.59
210	483.15	19.04	19.04
220	493.15	18.51	18.51
230	503.15	17.73	17.73
240	513.15	17.30	17.30
250	523.15	16.97	16.97
260	533.15	16.63	16.63
270	543.15	15.90	15.90
280	553.15	15.54	15.54
290	563.15	15.01	15.01
300	573.15	14.71	14.71
310	583.15	14.29	14.29
320	593.15	13.98	13.98

4.1.4 Viscosity

Viscous flow and laminar turbulence were activated in the modelling software. Viscosity was defined as a function of temperature because viscosity of polymers is known to change with temperature [30]. The data used in this analysis were obtained from previous work by Zitzenbacher *et al*., [30], as outlined in Table 5. It was found challenging to run simulations using the exact values of viscosity shown in the third and fourth columns in Table 5 that were obtained from the foregoing reference, as this caused the software to generate errors. The Flow 3D software used here is meant for simulating metals, which have much lower values of viscosities compared to polymers. Therefore, the values of viscosity shown in the fourth columns in Table 5, were reduced by a factor of 10^4 to enable the software to run the simulations, following a trial and error method. The software gave an error message when the values of viscosity were reduced by factors of 10^3 and 10^2. Thus, it is expected that these changes would reduce the accuracy of the results obtained from simulation. Hence, the observation that Flow 3D software is not suitable for investigating the sintering phase in PLS.

Table 5. Zero shear viscosity for PP at different temperatures according to Zitzenbacher et al., [30]

Temperature (℃)	Temperature (K)	Viscosity (Pa.s)	Viscosity (g/cm/s)	Adjusted values
185	458	3777.92	37779.2	3.77792
200	473	2628.46	26284.6	2.62846
210	483	2210.41	22104.1	2.21041
220	493	1719.04	17190.4	1.71904

4.1.5 Specific heat capacity

The values of specific heat capacity of PP were taken from a previous study by Vargha-Butler *et al*., [31] as shown in Table 6.

Table 6. Values of specific heat capacity of PP at different temperatures

Temperature (℃)	Temperature (K)	Specific heat (kJ/kg K)	Specific heat (erg/g/K)
27	300	1.680	1.68e+06
37	310	1.782	1.782e+06
47	320	1.843	1.843e+06
57	330	1.978	1.978e+06
67	340	2.051	2.051e+06
77	350	2.120	2.120e+06
87	360	2.159	2.159e+06

4.1.6 Thermal conductivity

The values of the thermal conductivity for PP at different temperatures were read from a graph obtained from a previous work by Dawson *et al*. [32]. These values are outlined in Table 7.

Table 7. Values of thermal conductivity of PP at different temperatures

Temperature (℃)	Temperature (K)	Thermal conductivity (W/mK)	Thermal conductivity (erg/cm/s/K)
50	323	0.24	24000
100	373	0.25	25000
150	423	0.18	18000
200	473	0.21	21000
250	523	0.22	22000

4.1.7 Other properties

The liquidus temperature, solidus temperature, and latent heat of fusion for PP (Ultrasint PP nat 01 powder) was obtained from a differential scanning calorimetry (DSC) experiment that was carried out at the QwaQwa Campus of the University of the Free State in South Africa as 143.6 °C, 95.2 °C, and 65.8 J/g, respectively [39]. The DSC was performed using a DSC 6000 PerkinElmer equipment. The heating and cooling cycles in this experiment were applied at a temperature rate of 10.00 *℃/min*. Heating was done from 30.0 ℃ to 180.0 ℃, whereas cooling was done from 180.0 ℃ to 30.0 ℃, with a hold of 1.0*min* at 30.0 ℃. Approximately 5.0 *mg* samples were used, and experimentation undertaken in an environment of nitrogen.

4.2 Boundary conditions

The boundaries of x-min, x-max, y-min, y-max, and z-min were set to wall type boundary and the temperature set to 403.15 K (extraction chamber temperature, which is normally lower than the build chamber temperature), while the temperature at the boundary, z-max, was set to 428.15 K (build chamber temperaturge) which is close to the melting point (433.15 K) of the material considered in this study. The known requirement that the building and extraction chamber temperatures should be maintained at a temperature close to the melting point of the polymer to reduce shrinkage [2] was imposed in the present work. Moreover, as is the norm, the build chamber temperature was kept higher than the extraction chamber temperature.

4.3 Initials conditions

New conditions were used to add a fluid region, above which the powder bed from spreading simulation (Study 5) was populated. This the fluid region was created to serve as a bed for the particles of powder, as shown in Figure 6. The second region (domain for the particles) was created manually using primitive features.

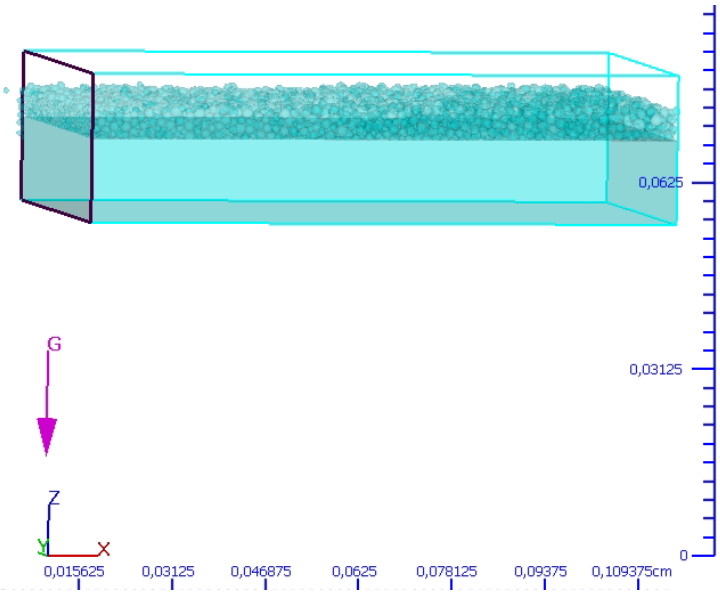

Figure 6. A fluid bed for the particles of powder lying on top of a fluid region

4.4 Flow 3D Weld

The rest of the simulation set-up was undertaken in Flow-3D weld. Here, settings of the laser beam were entered under the heat sources icon. Some of the settings included, the position of the laser beam, shape of the laser beam, radius of the lens, radius of the laser spot, setting of the scanning direction, power of the laser beam, and scanning velocity of the laser beam. Table 8 outlines crucial settings of the laser beam that were considered in this analysis. The position of the laser beam and scanning direction are shown in the results section. Similarity, the power and the scanning velocity of the laser beam were varied as illustrated in the results section

Table 8. Laser beam setting considered in this analysis

Laser beam parameter	**Prescribed value**
Shape of the laser beam	Gaussian distribution
Radius of the lens	0.005 cm
Radius of the laser spot	

5. RESULTS FROM THE NUMERICAL MODELLING

The numerical simulations performed using Flow 3D software showed different morphologies of melt pools obtained using different values of the process-parameters of laser power and scanning-speed. According to Yeh *et al*., [33], the size and appearance of the melt pool are essential indicators of the quality of final parts and simulations referencing these two factors (process parameters) can be employed to optimise process-parameters. Riedlbauer *et al*. [34] noted that the size of a melt pool can be used to estimate a suitable hatch distance by considering the size of the width. The authors added that the depth of a melt pool is an indicator of the quality of bonding between successive layers, which can be used to establish suitable laser power and speed of scanning. The output results considered in this analysis were the width and depth of melt pools (shown in Figure 7) for tracks printed with different process-parameters.

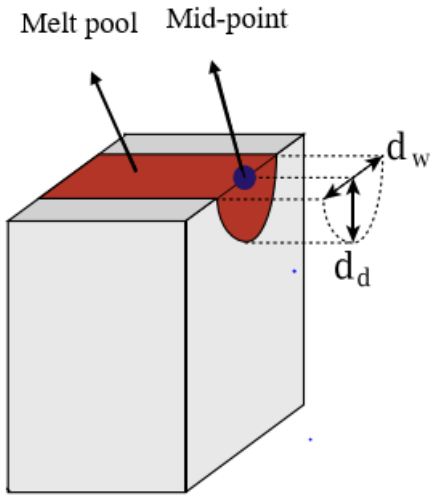

Figure 7. Width and depth of a melt pool (Riedlbauer et al., 2014)

In this figure:

d_w = width of a melt pool

d_d = depth of a melt pool

The depth of a melt pool is significant because it is an indicator of the quality of fusion between consecutive layers, which partly determines the mechanical performance of printed parts [3]. The simulated depths of a melt pools can be used to establish suitable values of layer-thickness. Shen *et al*. [35] stated that the depth of a melt pool should be greater than the thickness of a single layer but lower than twice the height of a single layer, to ensure sufficient interlayer fusion without causing re-melting. While this is a concern below the lower limit, lack of sufficient softening of previous layers is the concern above the upper limit. Though Lupone *et al*., [3] observed that re-melting can cause unwanted thermal stresses in printed parts or degradation of powder, the former is the case not due to re-melting but rather creation of any temperature gradient The width of a melt pool is useful for pre-process settings because it is used as a reference in setting hatch spacing to ensure good bonding between adjacent tracks. It can also be used to determine printing time based on the entire breadth of parts supposed to be printed. Figure 8 illustrates what can be considered as an optimal melt pool track, with regard to the depth-to-width ratio and shape of the track cross-section (elliptical).

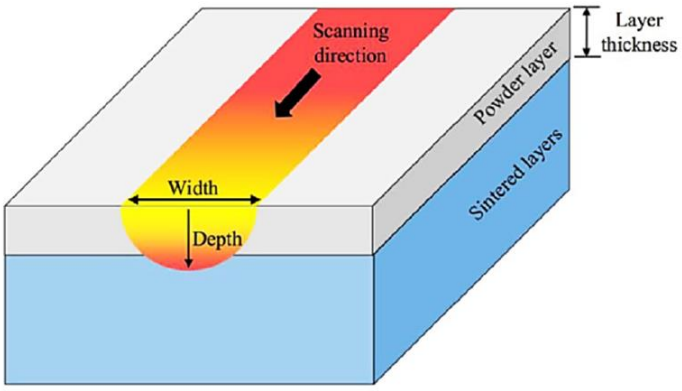

Figure 8. Suitable melt pool morphology [depth and width] [35]

The formation and evolution of a melt pool in the PLS occurs due to the interaction of a laser beam and a polymeric material. The properties of the melt pool are subject to the process-parameters of PLS. Lupone *et al*. [3] stated that laser power, scanning-speed, and hatch distance are the most crucial process-parameters that influence the characteristics of melt pool. The stability of a melt pool is an essential aspect because it influences the quality of printed parts [36]. Hence, the properties of a melt pool can be used to assess the suitability of different settings of process-parameters. Results from the simulation of single tracks can be utilised to optimise the laser power and scanning-speed by assessing depth and width of the melt pool.

In a previous study [23], suitable process-parameters for Ultrasint PP nat 01 were identified and outlined as shown in Table 9. These values were used as the basis for selecting the process-parameters for the numerical analysis.

Table 9. Recommended process-parameters for Ultrasint PP nat 01

Process parameter	Value
Laser power	44.8 W
Scanning-speed	4500 mm/s

Different scanning velocities (500 mm/s, 3000 mm/s, and 4500 mm/s) and laser powers (5 W, 25 W, 50W, and 75W) were considered in this analysis. Images obtained from the Flow 3D software were evaluated using ImageJ software to measure the depths and widths of the melt pools for single tracks simulated for different values of scanning-speed and laser power.

5.1 Values of depth and width of tracks that were simulated using different scanning-speeds

The values of depth and width of melt pools for tracks that were simulated using different scanning-speeds are outlined in Table 10. The laser powder was held at a constant value of 50W.

Table 10. Measured depths and widths of melt pools for single tracks simulated using different values of scanning-speeds

Laser scanning-speed (mm/s)	**500**	**3000**	**4500**
Depths of the melt pools (µm)	550	76.67	66.67
Widths of the melt pools (µm)	680	372.50	235.45
Ratios of depth to width of the melt pools	0.81	0.21	0.28

Figures 9 and 11 show graphical representations of the depths and widths of melt pools for single tracks simulated using different values of scanning-speed, respectively. Figures 10 and 12 show the cross-section and surface images of melts pools that were obtained from simulation. It is evident from the first two figures that the widths and depths of melt pools decreased with increasing scanning-speed. These results are in agreement with the findings of [19, 33, 37].

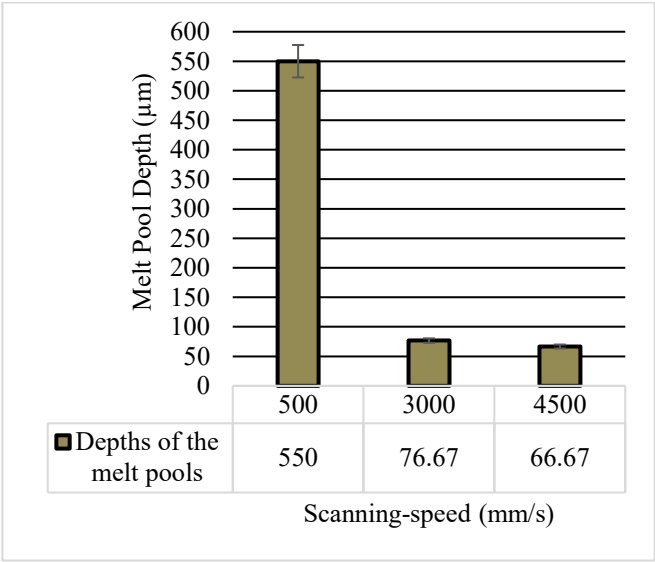

Figure 9. Changes in the depths of melt pools with scanning-speeds at a constant laser-power

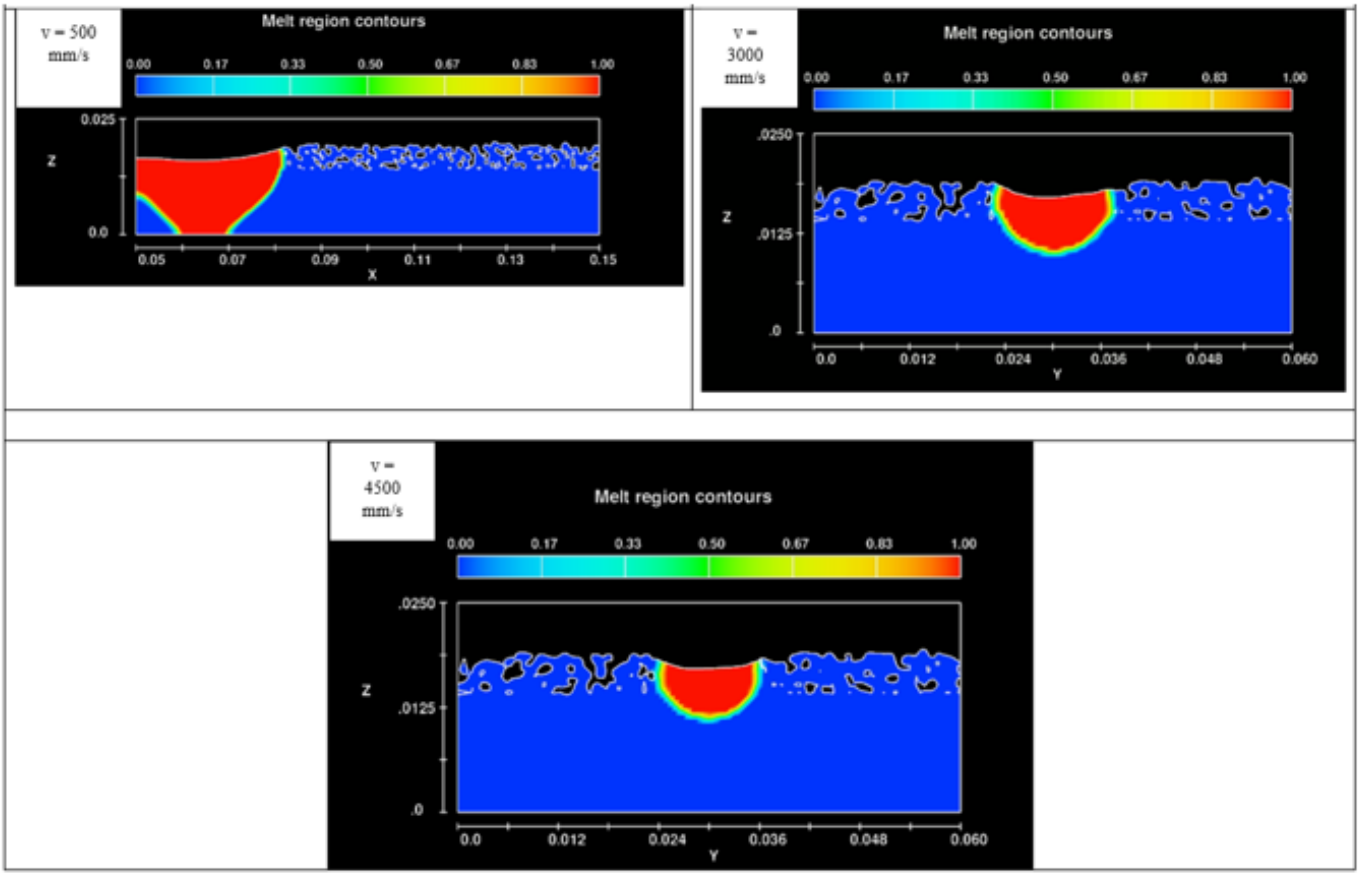

Figure 10. Images of the cross-section of melt pools simulated using different scanning-speeds at a constant laser-power

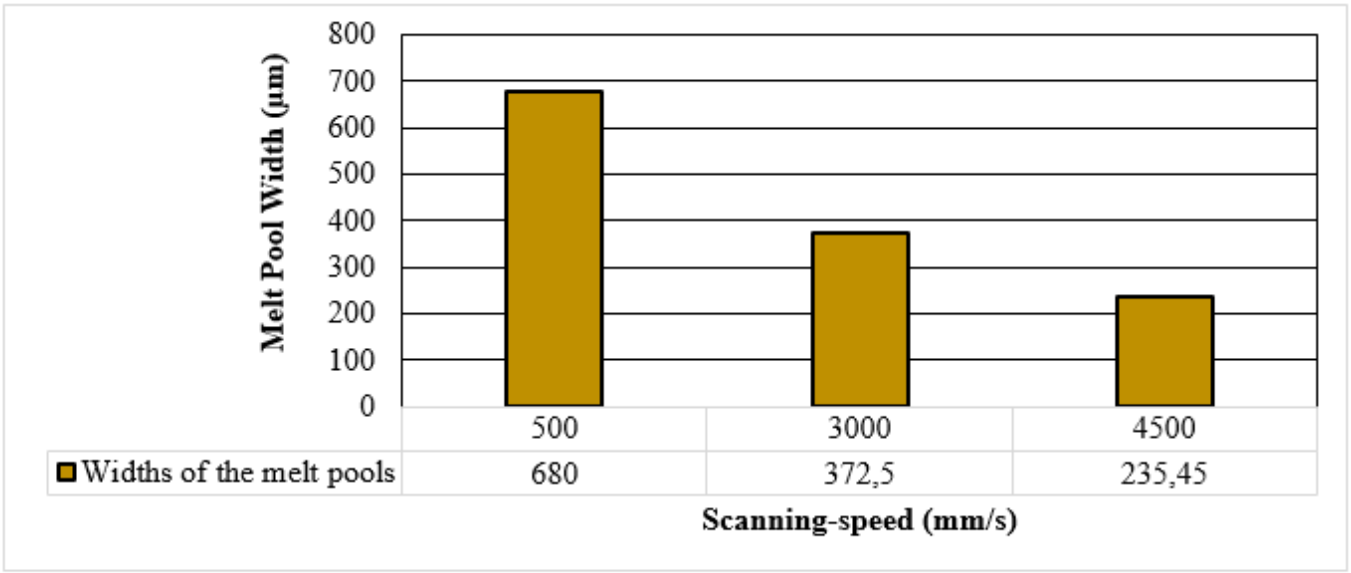

Figure 11. Changes in the widths of melt pools with scanning-speeds at a constant laser-power

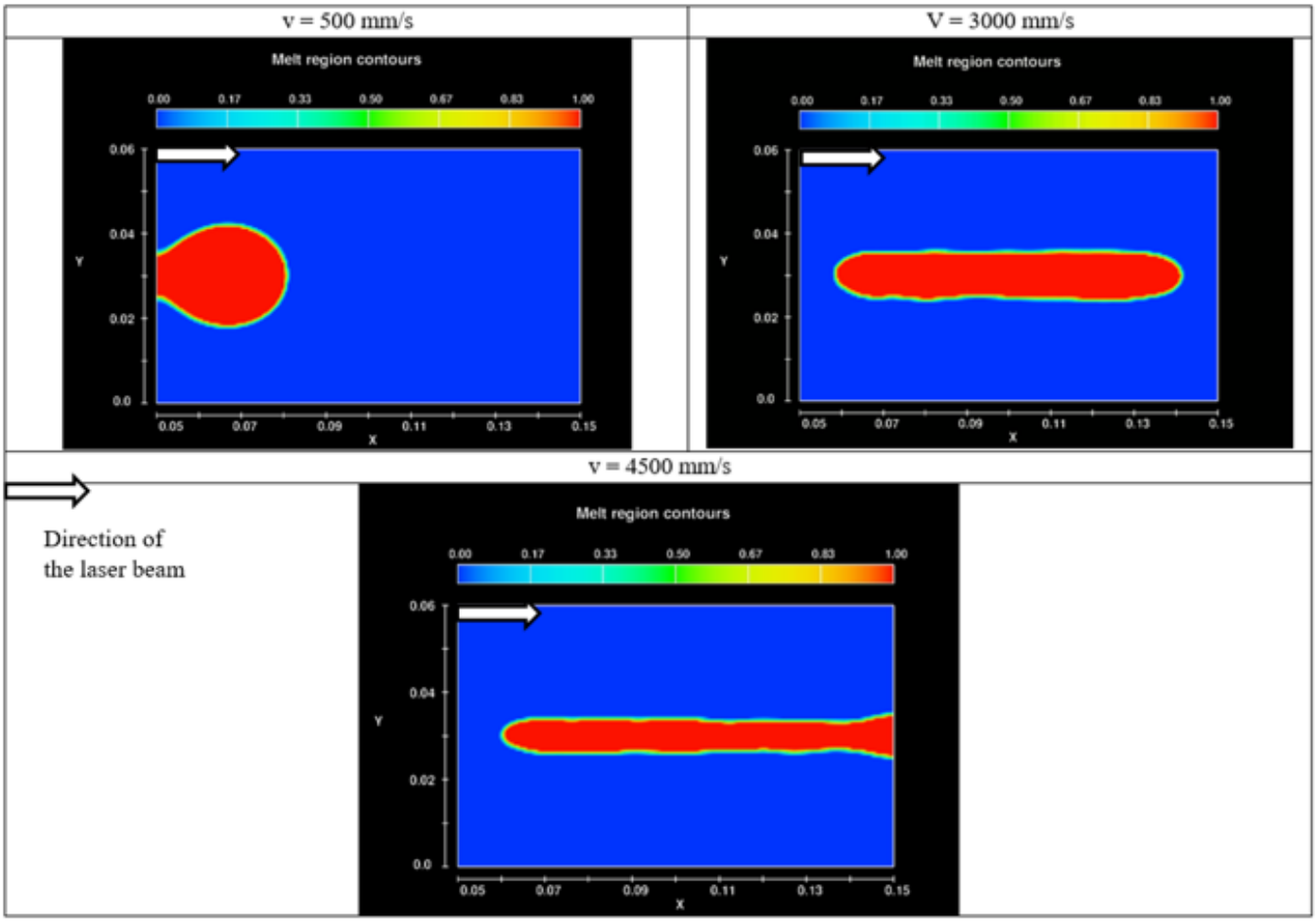

Figure 12. Images of the top surfaces of melt pools simulated using different scanning-speeds at a constant laser-power

The results presented in the preceding table, two graphs and figures indicate a relationship between scanning-speed and print distance, track widths and depths. When the lowest scanning-speed of 500 mm/s was used, the set simulation time expired before the laser beam moved a significant distance along the x-direction. Hence, the localised sintering observed in Figure 12, causing a high depth of penetration in the z-direction (depth). Scanning at the highest speed (4500 mm/s) resulted in the formation of a narrow track. The beam also moved out of the defined domain. A scanning-speed of 3000 mm/s resulted into a desirable shape of the track in terms of depths and widths, as illustrated in Figures 10 and 12. These findings illustrate that the Flow 3D software can be used to optimise the scanning-speed in PBF. However, this was not pursued for this particular study because of the suspected inaccuracies due to the adjusted values of viscosity, which does not reflect the actual values for Ultrasint PP nat 01 material.

5.2 Values of depth and width for single tracks that were simulated using different values of laser power

The obtained data was recorded in Table 11 and plotted in Figures 13 and 15 to present melt pool depth and width, respectively. Figures 14 and 16 present the cross-sections and top surfaces, respectively, of melt pools for tracks that were simulated at different values of laser power. The scanning speed was held at a constant value of 3000 mm/s.

Table 11. Measured values of depths and widths of melt pools for single tracks that were simulated using different values of laser power

Laser power (W)	Depths of the melt pools (µm)	Widths of the melt pools (µm)	Ratios of depth to width of the melt pools
5	22.50	158.31	0.14
25	72.00	378.75	0.19
50	92.50	523.75	0.18
75	152.50	847.78	0.18

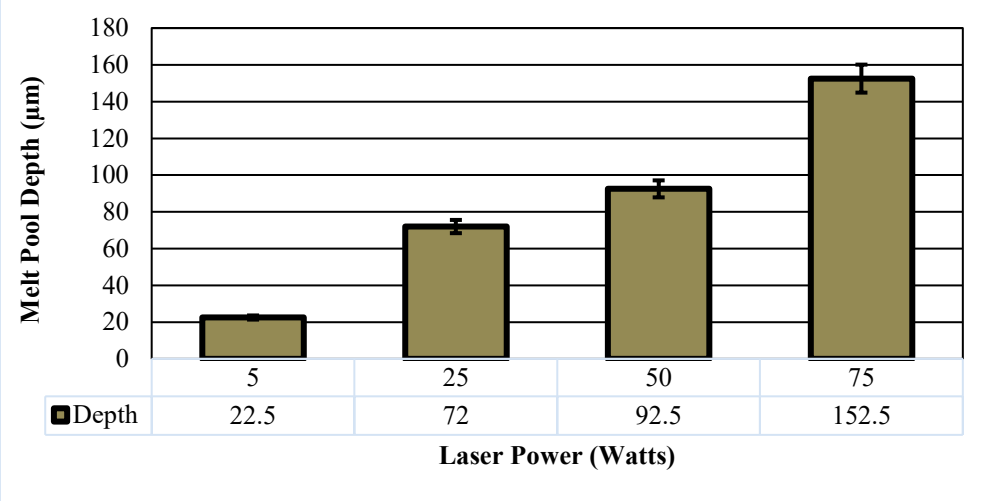

Figure 13. Changes of the depths of melt pools with the magnitude of laser power at a constant scanning-speed

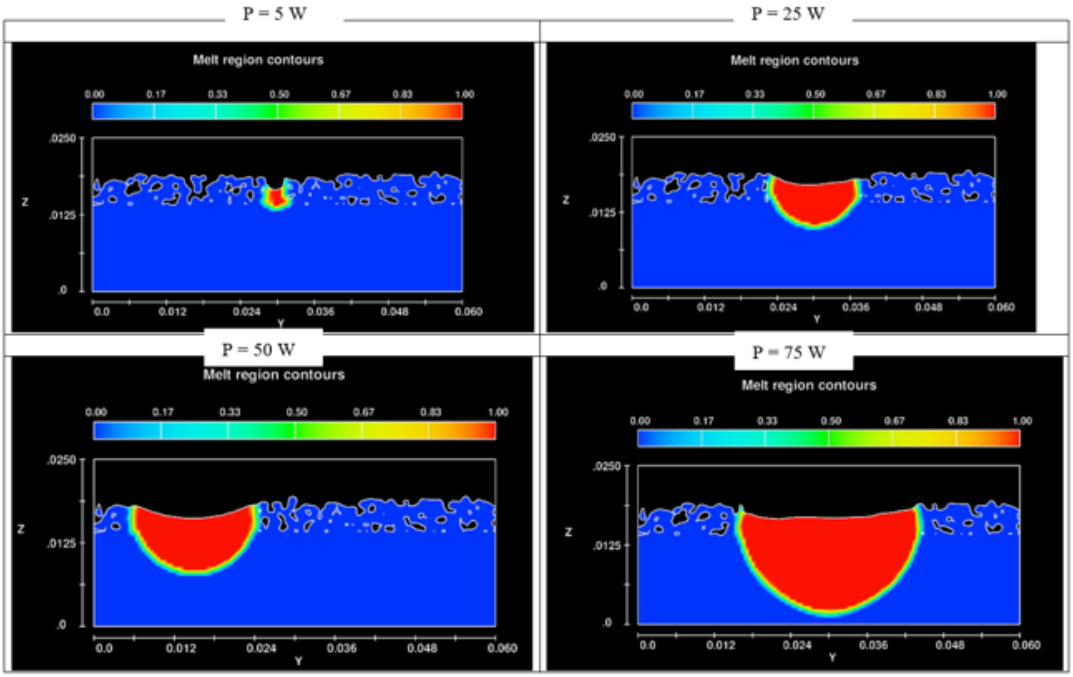

Figure 14. Images of the cross-sections of melt pools of single tracks that were simulated using different values of laser power at a constant scanning-speed

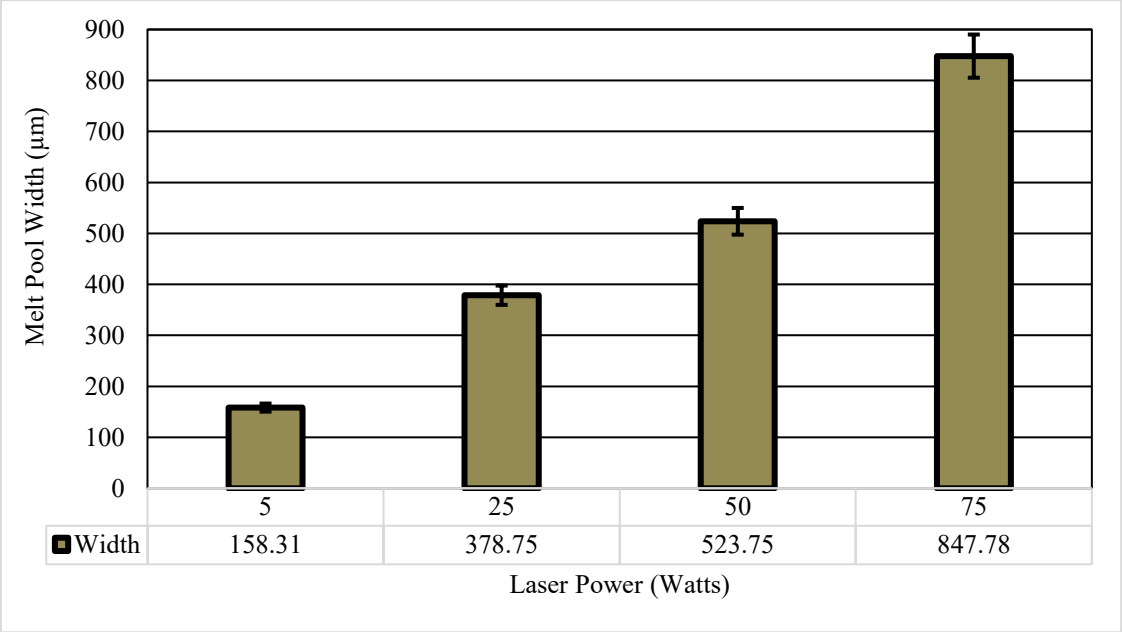

Figure 15. Changes of the widths of melt pools with the magnitude of laser power at a constant scanning-speed

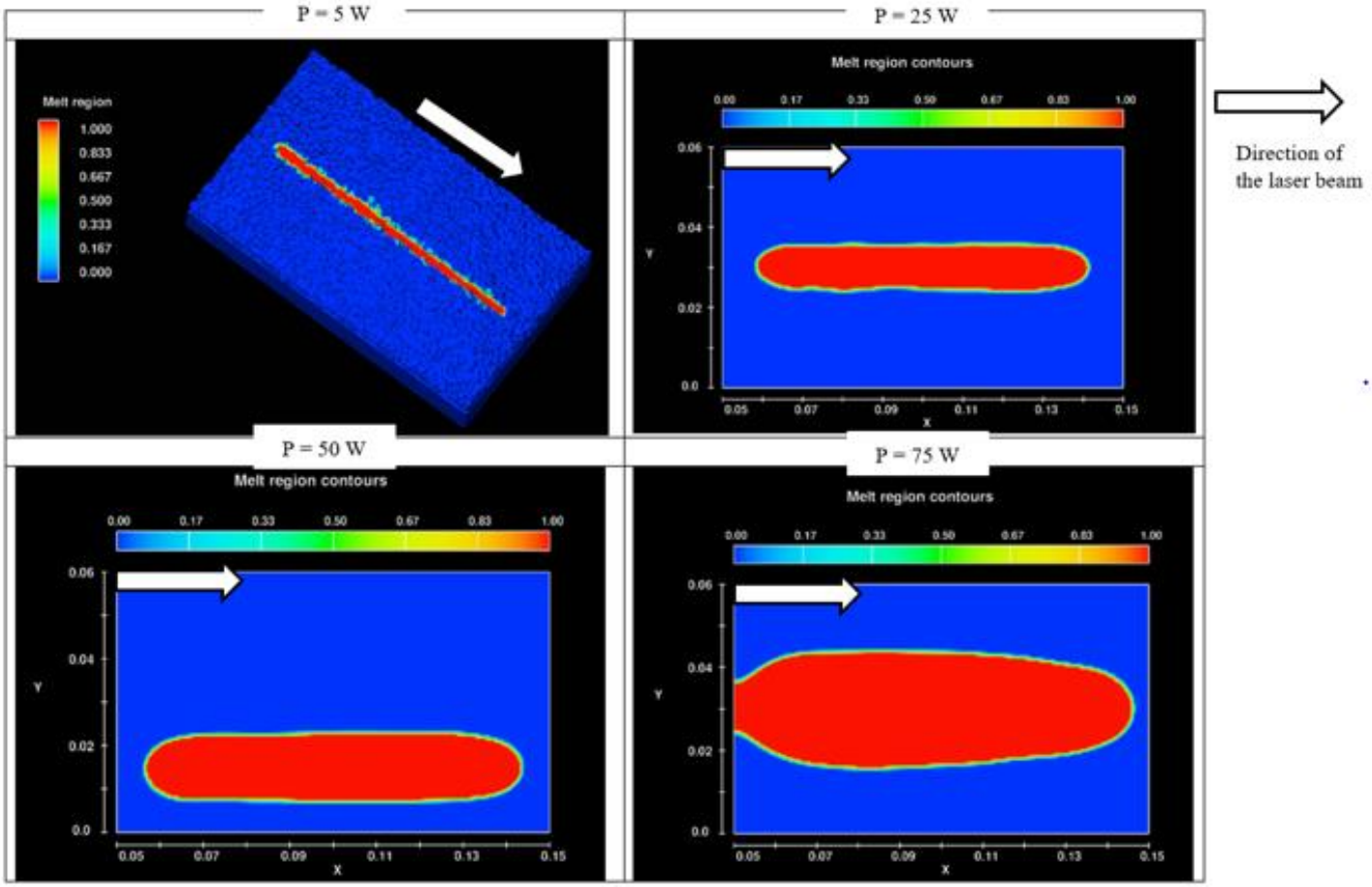

Figure 16. Images of the top surfaces of melt pools of single tracks simulated using different values of laser power at a constant scanning-speed

Figures 13 and 14 illustrate that the depth and width of the melt pool increases with increasing magnitude of the laser power. These results are in agreement with findings from the study by Peyre *et al*. [38], which showed that the depth of fusion of PA12 and PEKK increased with increasing laser power based on both simulation and experimental findings. According to Li *et al*. (2020), increasing laser power, caused the depth of the melt pool for PA6 to increase based on numerical and experimental analysis. Majeed *et al*. [37] confirmed that the depth of the melt pool increases with increasing laser power. Figures 15 and 16 indicate that the width of the melt pool increases with laser power. It is also evident that the shape of the melt pool is subject to laser power. Low magnitudes of laser power result into narrow melt pools, similar to the one obtained for a laser power of 5 W shown in Figure 16. This will lead to considerable printing time for parts, which is undesired for large-scale production. On the other hand, the higher laser power of 25 W and extremely high laser power of 75 W resulted in irregularly shaped melt pools along their lengths, as shown in Figure 16. Both these shapes are undesirable as they limit effective bonding of adjacent tracks and might cause weaknesses of the final printed parts. It is advisable to establish a laser power that provides a melt pool with a large enough width to ensure reduced printing time and one that yields a melt pool with a uniform width along the length of tracks. A substantial depth of the melt pool is also desirable to ensure proper bonding between adjacent layers. The track built at a laser power of 50 W as seen in Figures 14 and 16, is wide and has a continuous outline for most of its length. Hence, a laser power of about 50 W can be taken to be the most suitable for printing for this particular case.

6. CHALLENGES OF SIMULATING THE SINTERING PHENOMENON IN PLS USING FLOW 3D

Significant challenges were experienced when simulating PLS using Flow 3D software due to lack of material-properties, which had to be entered manually. The material library of the software does not contain pre-defined properties for polymers. Therefore, it was impossible to run simulation using the actual values of viscosity for the polymeric material considered in the analysis. The Flow 3D software is meant to simulate processing of metals, which have much lower values of viscosity compared to polymers. According to Yeh *et al*., [33], polymers have high viscosity, low flowability, and low conductivity, which causes slow evolution of the melt region. Peyre *et al*. [38], noted that the viscosity of polymers is almost 10^6 times greater than viscosity of metals. The values of viscosity for the polymeric material considered in this study were reduced to allow simulation to proceed. Hence, the Flow 3D software might not be suitable for running simulations when optimising process-parameters for new polymeric materials.

7. CONCLUSIONS

The following conclusions arose from the results presented, analysed and discussed in this study:

- ✓ The degree of fusion or coalescence of particles of polymer increased with temperature once the melting point of the material was attained and full fusion of particles that were in contact was achieved at 170 °C.
- ✓ Therefore, the fusion or coalescence behaviour of particles of polymers during sintering is subject to the total energy absorbed by them.
- ✓ The total energy absorbed by particles of polymer due to preheating and their interaction with the laser beam influences the value of the parameter (Ω) proposed in this work for their degree of fusion or coalescence.
- ✓ The dimensions of printed tracks are predicated on linear energy density given the observations from numerical simulation that the depths and widths of melt pools increased with increasing laser power and reduced with increasing scanning speed.
- ✓ The Flow 3D software cannot in its present form provide accurate optimal process-parameters for polymers, since it is developed solely for analysing metals.

8. CREDIT AUTHORSHIP CONTRIBUTION STATEMENT

Fredrick M Mwania: conceptualisation, formal analysis, investigation, methodology, validation, visualization, writing (original draft), writing (review and editing). **Maina Maringa**: formal analysis, investigation, validation, writing (review and editing), supervision. **Jacobus van der Walt**: formal analysis, investigation, validation, writing (review and editing), supervision, funding acquisition.

9. DECLARATION OF COMPETING INTEREST

The authors have no conflicting interests.

10. DATA AVAILABILITY

Data will be made available on request.

11. REFERENCES

[1] Han, W., Kong, L. and Xu, M., Advances in selective laser sintering of polymers. *International Journal of Extreme Manufacturing*, Vol.4, No.4, pp.1-37, (2022).

[2] Goodridge, R.D., Tuck, C.J. and Hague, R.J.M., Laser sintering of polyamides and other polymers. *Progress in Materials science*, Vol.57, No.2, pp.229-267, (2012).

[3] Lupone, F., Padovano, E., Casamento, F. and Badini, C., Process phenomena and material-properties in selective laser sintering of polymers: A review. *Materials*, Vol.15, No.1, pp.1-37, (2021).

[4] Franco, A., Lanzetta, M. and Romoli, L., Experimental analysis of selective laser sintering of polyamide powders: an energy perspective. *Journal of Cleaner Production*, Vol.18, No. (16-17), pp.1722-1730, (2010).

[5] Osmanlic, F., Wudy, K., Laumer, T., Schmidt, M., Drummer, D. and Körner, C., Modeling of laser beam absorption in a polymer powder bed. *Polymers*, Vol.10, No.7, pp.784-795, (2018).

[6] Hejmady, P., van Breemen, L.C., Anderson, P.D. and Cardinaels, R., Laser sintering of polymer particle pairs studied by in situ visualization. *Soft Matter*, Vol.15, No.6, pp.1373-1387, (2019).

[7] Schuffenhauer, T., Stichel, T., & Schmidt, M., Experimental determination of scattering processes in the interaction of laser radiation with polyamide 12 powder. *Procedia CIRP*, Vol.94, pp.85-88, (2020).

[8] Zhang, L., Boutaous, M.H. and Xin, S.H., 3D Modeling of Polymer Selective Laser Sintering Process: Laser-Polymer Interaction Modeling. *Key Engineering Materials*, Vol.92, pp.349-357, (2022).

[9] Alvarez, J.E., Nijkamp, A.H., Cheng, H., Luding, S. and Weinhart, T., Contact rheological DEM model for visco-elastic powders during laser sintering. *Granular Matter*, Vol.26, No.2, pp.1-14, (2024).

[10] Mokrane, A., Boutaous, M.H. and Xin, S., Process of selective laser sintering of polymer powders: Modeling, simulation, and validation. *Comptes Rendus. Mécanique*, Vol.3 46, No.11, pp.1087-1103, (2018).

[11] Gusarov, A.V. and Smurov, I., Modeling the interaction of laser radiation with powder bed at selective laser melting. *Physics Procedia*, Vol.5, pp.381-394, (2010).

[12] Yaagoubi, H., Abouchadi, H. and Janan, M.T., Review on the modeling of the laser sintering process for Polyamide 12. *E3S Web of Conferences*, Vol. 234, pp. 00006 – 00011, (2021).

[13] Yaagoubi, H., Abouchadi, H. and Janan, M.T., Simulation of the Heat Laser of the Selective Laser Sintering Process of the Polyamide12. *E3S Web of Conferences*, Vol. 297, pp. 01050-01055, (2021).

[14] Li, M., Zhao, Z., Yang, Q., Wei, Y. and Li, J., Investigation of the effect of laser energy density on selective laser sintering of PA12 using a multi-physics field simulation method. *The International Journal of Advanced Manufacturing Technology*, Vol.129, No.5, pp.1987-1998, (2023).

[15] Tang, X., Chen, X., Sun, F., Liu, P., Zhou, H. and Fu, S., The current state of CuCrZr and CuCrNb alloys manufactured by additive manufacturing: A review. *Materials & Design*, Vol.224, pp.1-32, (2022).

[16] Hofland, E.C., Baran, I. and Wismeijer, D.A., Correlation of process-parameters with mechanical properties of laser sintered PA12 parts. *Advances in materials science and engineering*, Vol.2017, No.1, pp.4953173, (2017).

[17] Pavan, M., Faes, M., Strobbe, D., Van Hooreweder, B., Craeghs, T., Moens, D. and Dewulf, W., On the influence of inter-layer time and energy density on selected critical-to-quality properties of PA12 parts produced via laser sintering. *Polymer testing*, Vol.61, pp.386-395, (2017).

[18] Li, E., Wang, L., Zou, R., Yu, A. and Zhou, Z., Investigation of laser-powder interaction in laser powder bed fusion process in additive manufacturing. In *EPJ Web of Conferences* (Vol. 249, p. 12002). EDP Sciences, (2021).

[19] Li, M., Han, Y., Zhou, M., Chen, P., Gao, H., Zhang, Y. and Zhou, H., Experimental investigating and numerical simulations of the thermal behavior and process optimization for selective laser sintering of PA6. *Journal of*

Manufacturing Processes, Vol.56, pp.271-279, (2020).
[20] Yehia, H.M., Hamada, A., Sebaey, T.A. and Abd-Elaziem, W., Selective Laser Sintering of Polymers: Process-parameters, Machine Learning Approaches, and Future Directions. *Journal of Manufacturing and Materials Processing*, Vol.8, No.5, pp.197-225, (2024).
[21] Benedetti, L., Brulé, B., Decraemer, N., Evans, K.E. and Ghita, O., Evaluation of particle coalescence and its implications in laser sintering. *Powder technology*, Vol.342, pp.917-928, (2019).
[22] Brighenti, R., Cosma, M. P., Marsavina, L., Spagnoli, A., & Terzano, M., Laser-based additively manufactured polymers: A review on processes and mechanical models. *Journal of Materials Science*, Vol.56, No.2, pp.961-998, (2021).
[23] Wu, L., Mwania, F.M., Van der Walt, J.G. and Koen, W., An evaluation of the suitability of a new polypropylene powder for powder bed fusion additive manufacturing. *MATEC Web of Conferences*, Vol. 388, pp. 06003-06012, (2023).
[24] Wilkinson, R.W. and Dole, M., Specific heat of synthetic high polymers. X. Isotactic and atactic polypropylene. *Journal of Polymer Science*, Vol.58, No.166, pp.1089-1106, (1962).
[25] Yan, X., Cayla, A., Devaux, E. and Salaün, F., Microstructure evolution of immiscible PP-PVA blends tuned by polymer ratio and silica nanoparticles. *Polymers*, Vol.10, No.9, pp.1031-1048, (2018).
[26] Mwania, F.M., Maringa, M. and van der Walt, J., Determining the best exposure volumetric energy density for Diapow PP MF polypropylene from a study of its different dynamic mechanical properties. *Results in Materials*, Vol.21, Pp.100548-100556, (2024).
[27] FLSMIDTH (n.d). Gases - Specific Heat Capacities and Individual Gas Constants. Retrived from https://ceimusb.files.wordpress.com/2015/09/calor_especifico_de_gases.pdf (22/07/2024).
[28] Lazar, A., Croitoru, C., Tierean, M.H. and Baltes, L.S., October. Thermal and Thermorheologic Characterization of Different Polyolefin Waste Fractions. I*Materials Science Forum*, Vol. 907, pp. 74-79, (2017).
[29] Funke, Z., Schwinger, C., Adhikari, R. and Kressler, J., Surface tension in polymer blends of isotactic poly (propylene) and atactic polystyrene. *Macromolecular Materials and Engineering*, Vol.286, No.12, pp.744-751, (2001).
[30] Zitzenbacher, G., Dirnberger, H., Längauer, M. and Holzer, C., Calculation of the contact angle of polymer melts on tool surfaces from viscosity parameters. *Polymers*, Vol.10, No.1, pp.38-50, (2017).
[31] Vargha-Butler, E.I., Neumann, A.W. and Hamza, H.A., Specific heats of polymer powders by differential scanning calorimetry. *Canadian Journal of Chemistry*, Vol.60, No.14, pp.1853-1856, (1982).
[32] Dawson, A., Rides, M., Urquhart, J. and Brown, C.S., Thermal conductivity of polymer melts and implications of uncertainties in data for process simulation. *Cerca con Google*, pp.1-17, (2000).
[33] Yeh, H.P., Bayat, M., Arzani, A. and Hattel, J.H., Accelerated process parameter selection of polymer-based selective laser sintering via hybrid physics-informed neural network and finite element surrogate modelling. *Applied Ma thematical Modelling*, Vol.130, pp.693-712, (2024).
[34] Riedlbauer, D., Drexler, M., Drummer, D., Steinmann, P. and Mergheim, J., Modelling, simulation and experimental validation of heat transfer in selective laser melting of the polymeric material PA12. *Computational Materials Science*, Vol.93, pp.239-248, (2014).
[35] Shen, F., Yuan, S., Chua, C.K. and Zhou, K., Development of process efficiency maps for selective laser sintering of polymeric composite powders: Modeling and experimental testing. *Journal of Materials Processing Technology*, Vol.254, pp.52-59, (2018).
[36] West, C. and Wang, X., Modeling of selective laser sintering/selective laser melting. *Laser 3D Manufacturing IV*, Vol. 10095, pp.1009506-1009513, (2017).
[37] Majeed, M., Khan, H.M., Wheatley, G. and Situ, R., A numerical approach to assess the impact of the SLM laser parameters on thermal variables. *Journal of Additive Manufacturing Technologies*, Vol.1, No.3, pp.589-589, (2021).
[38] Peyre, P., Rouchausse, Y., Defauchy, D. and Régnier, G., Experimental and numerical analysis of the selective laser sintering (SLS) of PA12 and PEKK semi-crystalline polymers. *Journal of Materials Processing Technology*, Vol.225, pp.326-336, (2015).
[39] Mwania, F., Maringa, M. and van der Walt, J., Characterising Ultrasint PP Nat 01 Polypropylene to Examine Its Feasibility in

Powder Bed Fusion. *Powders*, Vol.4, No.3, pp.26, (2025).